Available online at www.sciencedirect.com
ScienceDirect
Proceedings of the Combustion Institute 31 (2007) 1319–1326
Proceedings of the Combustion Institute
www.elsevier.com/locate/proci

Measurement of flame surface density for turbulent premixed flames using PLIF and DNS

Johan Hult [a,*], Sara Gashi [a,b], Nilanjan Chakraborty [c], Markus Klein [d], Karl W. Jenkins [e], Stewart Cant [b], Clemens F. Kaminski [a]

[a] *Department of Chemical Engineering, University of Cambridge, Pembroke Street, Cambridge CB2 3RA, UK*
[b] *Department of Engineering, University of Cambridge, Trumpington Street, Cambridge CB2 1PZ, UK*
[c] *Department of Engineering, University of Liverpool, Brownlow Hill, Liverpool L69 3GH, UK*
[d] *Technische Universität Darmstadt, Institut für Energie- und Kraftwerkstechnik, Petersenstr. 30, D-64287 Darmstadt, Germany*
[e] *School of Engineering, Cranfield University, Bedfordshire MK43 0AL, UK*

Abstract

Results for flame surface density (FSD) in premixed turbulent flame kernels have been obtained from OH planar laser induced fluorescence (PLIF) and direct numerical simulations (DNS), and have been compared for similar values of global Lewis number and normalised turbulence intensity. Stoichiometric methane–air and lean hydrogen–air mixtures were studied, and the same post-processing techniques were employed for both experimental and DNS data in order to evaluate FSD statistics from spatial gradients of the reaction progress variable. Full 3D FSD statistics were obtained from the DNS data sets. Also, FSD statistics were obtained from two-dimensional cross-sections extracted from the DNS data sets which were found to be in qualitative agreement with the FSD statistics of PLIF data. The location of maximum FSD within the flame was found to be close to the middle of the flame brush for both methane–air and hydrogen–air flames, and was found to be slightly skewed about the middle of the flame brush for some methane–air flames. The PLIF data for both fuels showed a decrease in the maximum FSD with increasing turbulence intensity. This effect was not observed in the three-dimensional DNS analysis for methane–air flames, but was found to be consistent with both two-dimensional and three-dimensional analysis of the DNS data for hydrogen–air flames. The findings have been compared with the results of other experimental and DNS work reported in the literature and mechanisms have been suggested to explain the observed behaviour.

Keywords: Flame surface density; Turbulent premixed flames; DNS; PLIF

1. Introduction

Turbulent premixed combustion is becoming ever more important in technical applications such as gas turbine combustors where reduction of pollutant emissions demands close control of the stoichiometry. At the same time, fundamental information on premixed flames is required in order to improve understanding as well as the accuracy and fidelity of modelling for the design of industrial combustion systems. Over a broad range of operating conditions, turbulent premixed flames are known to consist of highly wrinkled

* Corresponding author. Fax: +44 1223 334 796.
E-mail address: jfh36@cheng.cam.ac.uk (J. Hult).

1540-7489/$ - see front matter
doi:10.1016/j.proci.2006.07.188

quasi-laminar sheet-like structures known as flamelets [1]. One of the most promising approaches to their modelling is based on the Flame Surface Density (FSD), which quantifies the surface area of the flamelet per unit volume [2,3]. The FSD approach has been formulated in the context of both Reynolds-Averaged Navier–Stokes (RANS) and Large-Eddy Simulation (LES) as a simple algebraic closure [4,5] or in terms of a modelled balance equation [6]. Many variants exist [7,8] and there are stochastic [9] and spectral [10] formulations. Data from Direct Numerical Simulations (DNS) for flame propagation in terms of FSD has already proved very illuminating [11,12], and significant progress has been made in the experimental determination of FSD [13,14].

The present work is aimed at comparing FSD statistics obtained from both DNS and experiment under similar normalised turbulent velocity fluctuations u'/S_L (where u' is the turbulent velocity fluctuation and S_L is the unstrained laminar flame speed) in the flamelet regime [1]. A turbulent premixed flame kernel configuration is used which has several advantages. Computationally, the flame remains far from any influence of the boundaries and there is no experimental geometry to consider. Experimentally, the turbulence can be well-controlled in terms of length scales and velocity fluctuation magnitudes, while maintaining isotropy and homogeneity [15,16]. A previous comparison between experiment and three-dimensional DNS [17] for flame kernels showed good agreement for curvature statistics. The main objectives of this paper are: (a) to explore the sensitivity of the nature of FSD variation (maximum value and profile shape) in response to u'/S_L; (b) to compare the FSD statistics obtained from 2D and 3D evaluations. It should be noted that only a qualitative comparison between DNS and experimental data is intended.

Here, FSD data has been obtained computationally from three-dimensional DNS calculations with single step chemistry, and experimentally from time resolved planar laser induced fluorescence (PLIF) measurements on spark ignited turbulent methane–air and hydrogen–air mixtures. Conditions for both DNS and experiment are similar with u'/S_L up to 10 for both, and with integral length scales (L_{11}) agreeing within an order of magnitude. Results for FSD are presented in the form of scatter plots obtained at different values of u'/S_L for both DNS and experiment, and there is good qualitative agreement between them.

2. Experimental details

The combustion cell (designed at ITV, University of Stuttgart) has a cylindrical constant volume, and is equipped with four high-speed rotors, which generate controlled degrees of turbulence in the mixture [16]. The turbulence intensity at different rotor speeds in the centre of the cell had previously been characterized using laser Doppler velocimetry [18]. Stoichiometric methane/air and lean hydrogen/air mixtures were ignited by two electrodes located in the centre of the cell.

PLIF of OH is known to be a good marker of burnt and unburned regions in premixed flames. Measurements were performed at the high speed imaging facility at Lund Institute of Technology [16]. A cluster of four Nd:YAG lasers was fired sequentially at high repetition rates and used to pump a dye laser. The frequency doubled output of the dye laser was tuned to the temperature insensitive $Q_1(8)$ transition in the $v''=0$, $v'=1$ band of the $A^2\Sigma^+ \leftarrow X^2\Pi$ system of OH, around 283 nm. The laser beam was formed into a sheet (height = 40 mm, width = 300 μm) using a cylindrical lens telescope. The resulting fluorescence in the $v'=0 \rightarrow v''=0$ and $v'=1 \rightarrow v''=1$ bands around 315 nm was collected at right angles with a high speed ICCD camera using an achromatic quartz lens. The dynamic resolution of the camera was 8 bit, and the chip size 576×384 pixels. The experimental resolution (both spatial resolution, and laser sheet thickness) was about 0.2 mm, which is comparable to the flame reaction zone thickness, and much smaller than the flame wrinkling observed in any of the cases studied here.

The PLIF images were corrected for background levels and laser sheet non-uniformities, and then binarised into burnt and unburnt regions based on the location of the maximum OH gradient. For each experimental condition, more than 30 individual events were recorded to allow statistical information to be retrieved.

3. Numerical scheme and configuration

Simulations were performed using the DNS code SENGA [19,20], which uses tenth order central differences to compute all spatial derivatives and an explicit low storage third-order Runge–Kutta method for time advancement. The fully compressible Navier–Stokes equations were solved together with an equation for the reaction progress variable c, and single step Arrhenius chemistry was implemented. The chemical reaction rate is given by:

$$\dot{w} = B^* \rho (1-c) \exp\left[-\frac{\beta(1-T)}{1-\alpha(1-T)}\right] \quad (1)$$

where the non-dimensional temperature T, Zel'dovich number β, and heat release parameter α are given by

$$T = \frac{\hat{T}-T_0}{T_{ad}-T_0}; \quad \alpha = 1-\frac{\rho_b}{\rho_0}; \quad \beta = \frac{E_a(T_{ad}-T_0)}{R^0 T_{ad}^2} \quad (2)$$

where $\hat{T}$ denotes the instantaneous dimensional temperature, T_0 is the initial temperature, T_{ad} is

the adiabatic flame temperature, ρ_0 and ρ_b are the fresh and burned gas densities, B^* is the pre-exponential factor, R^0 is the universal gas constant and E_a is the activation energy. In all cases the pre-exponential factor B^* is adjusted to result in a unity laminar unstrained flame speed S_L. The computational domain was a cube extending in each direction over 24 times the thermal flame thickness $\delta_{th} = (T_{ad} - T_0)/\mathrm{Max}|\nabla\hat{T}|$, and was resolved with 230 uniformly placed grid points on each side. All the velocities in DNS were non-dimensionalised with respect to S_L. The flame was initialised using a self-sustaining spherical laminar flame solution, and the turbulent motion was superimposed in order to specify the initial condition for DNS. The initial radius of the burned gas kernel corresponded to twice the thermal flame thickness. Details on initial and boundary conditions may be found elsewhere [20]. The Lewis number Le, heat release parameter $\tau = (T_{ad} - T_0)/T_0$, and turbulence intensity u'/S_L were chosen to match the experimental conditions. Parameters characterising the conditions for both experiment and simulation are presented in Table 1. All the simulations were carried out for at least two initial eddy turn-over times ($2L_{11}/u'$). For both methane–air and hydrogen–air flames the Zel'dovich number β was taken to be equal to 6. The combustion parameters characterising the flow situation, including Damköhler number $Da = (L_{11}/\delta_L) \times (S_L/u')$, Karlovitz number $Ka = t_F/t_\eta$ [1], and turbulent Reynolds number $Re_t = \rho_0 u' L_{11}/\mu_0$ for the DNS database are presented in Table 2, where t_F is the chemical time scale given in terms of mass diffusivity as $t_F = D/S_L^2$ and t_η is the Kolmogorov time scale. Before proceeding, it is important to note that there is some uncertainty in determining the ratio between the integral length scaleL_{11} and the laminar flame thickness $\delta_L = 1/\mathrm{Max}|\nabla c|$ for the present experimental data. It is estimated that L_{11}/δ_L is 6–8 times larger for the experimental data than for the DNS results, which is sufficient to allow for a qualitative comparison. Due to the uncertainty in the L_{11} and t_η values under experimental conditions, the values of Re_t and Ka are presented for the numerical simulations only in Table 2. The turbulent Reynolds number scales as $Re_t \sim (u'/S_L) \times (L_{11}/\delta_L) \times 1/Sc$ due to the scaling $\mu_0/\rho_0 \sim Sc(S_L\delta_L)$, where Sc is the Schmidt number. As a result of this, the experimental turbulent Reynolds numbers are expected to be about 10 times larger than those employed in the DNS, due to the difference in the L_{11}/δ_L ratio. By the same token, the Damköhler number Da is expected to be 6–8 times higher in the experiments, compared to those reported in Table 2.

In DNS it is necessary to provide adequate resolution of the flame structure, and experience suggest that this requires at least 10 grid points within the flame thickness. The computational cost for DNS for experimental L_{11}/δ_L becomes prohibitive in nature. As a result, smaller simulations have been attempted for the present study. Note that the hydrogen–air flames were simulated using a planar configuration for reasons of computational convenience. It is recognised that the propagation behaviour of statistically planar flames may differ from that of flame kernels, but it is expected that meaningful comparisons are still possible since the radii of the experimental hydrogen–air kernels were about 50 times larger than the flame thickness at the time of comparison.

4. FSD evaluation

The reaction progress variable was obtained from the experimental PLIF data in binarised form, whereas in the DNS database c varied smoothly

Table 1
Flame parameters

Fuel	ϕ	Le	τ	u'/S_L	L_{11}/δ_L (initial)
CH_4	1.00	0.98 (PLIF), 1.0 (DNS)	6.5	1.68 (PLIF), 1.78 (DNS)	1.70 (DNS)
CH_4	1.00	0.98 (PLIF), 1.0 (DNS)	6.5	3.51 (PLIF), 3.37 (DNS)	1.70 (DNS)
CH_4	1.00	0.98 (PLIF), 1.0 (DNS)	6.5	5.43 (PLIF), 5.26 (DNS)	1.70 (DNS)
H_2	0.58	0.34 (PLIF, DNS)	4.5	1.76 (PLIF, DNS)	0.77 (DNS)
H_2	0.58	0.34 (PLIF, DNS)	4.5	3.55 (PLIF, DNS)	0.77 (DNS)

Table 2
Dimensionless parameters (DNS data only)

Fuel	$Da = (L_{11}/\delta_L) \times (S_L/u')$	$Ka = t_F/t_\eta$	$Re_t = \rho_0 u' L_{11}/\mu_0$
CH_4	0.95	3.80	7.57
CH_4	0.50	9.52	14.30
CH_4	0.32	19.04	22.41
H_2	0.44	18.04	7.48
H_2	0.22	29.68	15.10

from zero to unity. The fine-grained FSD Σ' is defined as [1]: $\Sigma' = |\nabla c|\delta(c - c^*) = |\nabla H(c - c^*)|$ where $H(c - c^*)$ is a Heaviside function. In order to compare DNS with experiment, a reduced progress variable is defined as $c_{\mathrm{red}} = H(c - c^*)$ [11], such that $\Sigma' = |\nabla c_{\mathrm{red}}|$. In the context of RANS modelling the FSD is obtained by ensemble averaging $|\nabla c_{\mathrm{red}}|$ over directions normal to the mean direction of flame propagation according to:

$$\Sigma = \langle \Sigma' \rangle = \langle |\nabla c_{\mathrm{red}}| \rangle \text{ and } \bar{c} = \langle c_{\mathrm{red}} \rangle \tag{3}$$

where the averaging operation is performed on concentric spherical shells (in three dimensions) or circles (in two dimensions) around the centre of mass of each flame kernel. For the statistically planar flames the averaging is performed on planes parallel to the flame. The same post processing technique is used for both DNS and experimental data and is similar to that used previously [5,11,13]. For the purpose of three-dimensional analysis the FSD is evaluated as:

$$\Sigma = \left\langle \sqrt{(\partial c_{\mathrm{red}}/\partial x)^2 + (\partial c_{\mathrm{red}}/\partial y)^2 + (\partial c_{\mathrm{red}}/\partial z)^2} \right\rangle \tag{4}$$

whereas for the purpose of two-dimensional analysis in the $x_\alpha - x_\beta$ plane the FSD is evaluated as:

$$\Sigma = \left\langle \sqrt{(\partial c_{\mathrm{red}}/\partial x_\alpha)^2 + (\partial c_{\mathrm{red}}/\partial x_\beta)^2} \right\rangle \tag{5}$$

The distribution of c_{red} may be sensitive to the choice of c^*. Here, two different choices for c^* have been considered ($c^* = 0.5$ and $c^* = 0.8$, corresponding to the location of peak reaction rate in hydrogen–air and methane–air flames, respectively) and both have been found to give similar results.

5. Results and discussion

Figure 1 shows examples of experimentally observed and simulated flames which are compared in this paper. Black corresponds to unburned gases and white to burnt gases. The top row represents the binarised OH PLIF data, obtained from the centre plane of the combustion cell and the bottom row represents DNS data, for which both three-dimensional simulations and two-dimensional planes extracted from such simulations are shown.

In the first row of experimental flames for the stoichiometric methane–air case it can be seen that the kernel becomes less spherical and develops a more corrugated flame shape when the turbulence intensity is increased. As a comparison, the lean hydrogen–air kernels are seen to develop even more fine scale structure as a consequence of finger formation due to low Lewis number effects [11]. In the left part of the second row, showing a DNS case with Lewis number matching that of a stoichiometric methane–air mixture, the kernel becomes less spherical and develops more fine-scale structure at the front with increasing turbulence intensity, just as in the experiment. The right part of the second row shows a planar DNS with Lewis number corresponding to a lean hydrogen–air mixture. Small-scale structures are seen to develop in the higher turbulence case, as in the experiment.

Experimental data for the variation of FSD with Reynolds averaged reaction progress variable $\bar{c}$ for stoichiometric methane–air flames is shown in Fig. 2a–c for different u'/S_{L} values. Since the experimental data is based on two-dimensional cross-sections, corresponding DNS data based on two-dimensional slices are presented in Fig. 2d–f for similar u'/S_{L} values. It should be noted that all experimental and DNS FSD values presented in this paper are normalised by the flame thickness ($\Sigma\delta_{\mathrm{L}}$). The standard deviation of the evaluated FSD was found to be around 30% for both the PLIF and the DNS data shown in Fig. 2, which still allows for the qualitative comparison intended here. The normalised maximum value of FSD in the experimental data is found to be about six times smaller than that obtained from the DNS database. As the maximum

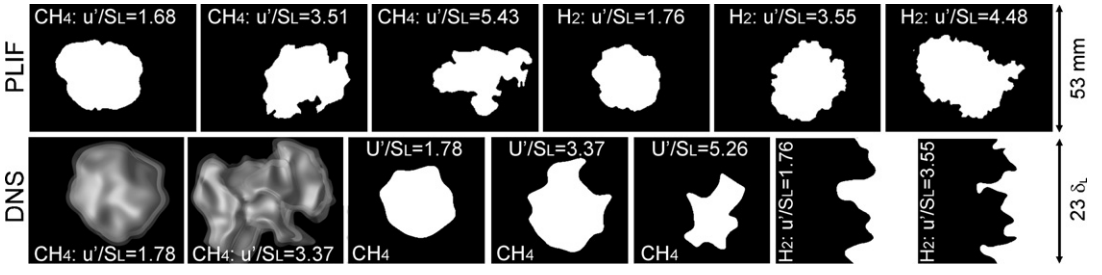

Fig. 1. Top row: binarised cross-sections of methane–air (images 1–3, time after ignition: 6.6, 5.7, and 4.8 ms, respectively) and hydrogen–air kernels (images 4–6, time after ignition: 1.8 ms), captured by OH PLIF. Bottom row: examples of 3D kernels simulated using DNS, corresponding to the methane–air case (images 1–2), along with cross-sections of such kernels (images 3–5) and of 3D DNS simulations of planar hydrogen–air flames (images 6–7). All DNS data corresponds to two eddy turnover times after initialisation.

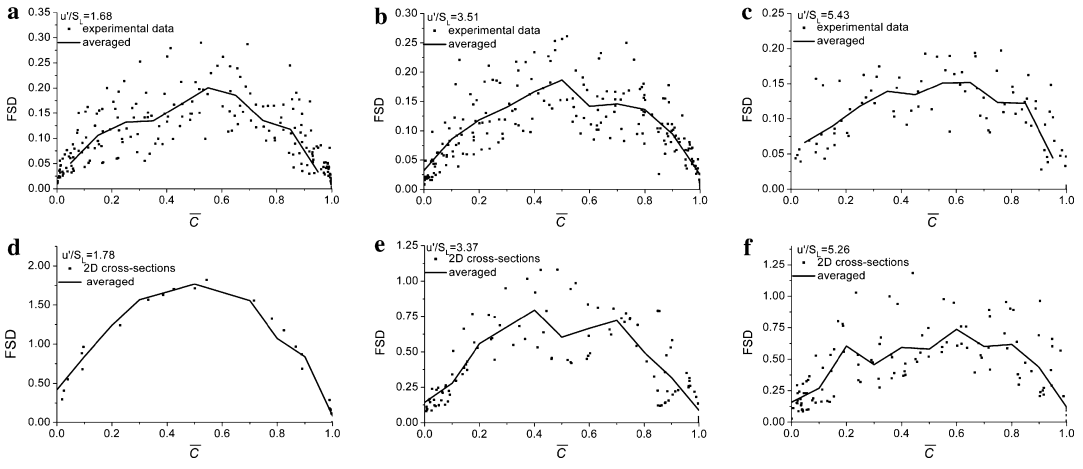

Fig. 2. Flame surface density of flame kernels propagating in stoichiometric methane–air mixtures of different turbulence intensity (top: experimental data; bottom: cross-sections of DNS data).

value of normalised FSD($\Sigma\delta_L$) scales with $(u'/S_L)\times(\delta_L/L_{11})$ [3–5,14], this deviation is expected due to the difference in the length scale ratio L_{11}/δ_L between the experiments and the DNS.

It can be seen from Fig. 2 that the FSD profile for some experimental and DNS cases is somewhat skewed about $\bar{c}=0.5$. Previous experimental studies [21–23] and DNS results [5,11,12,19,24] have indicated similar behaviour, which is not consistent with existing algebraic models [4], which predict maximum FSD at $\bar{c}=0.5$. In order to explain the observed behaviour it is instructive to consider the displacement speed S_d [1,12,19,24] as:

$$S_d = S_r + S_n - 2D\kappa_m, \quad \text{where}$$
$$S_r = \frac{\dot{w}}{\rho|\nabla c|} \quad \text{and} \quad S_n = \frac{\vec{N}\cdot\nabla(\rho D\vec{N}\cdot\nabla c)}{\rho|\nabla c|} \tag{6}$$

where κ_m is the local mean curvature given by $2\kappa_m=\nabla\cdot\vec{N}$ with the flame normal vector defined to be $\vec{N}=-\nabla c/|\nabla c|$, $\dot{w}$ is the reaction rate and D is the diffusion coefficient. Manipulation of the balance equation for the Favre-averaged progress variable $\tilde{c}$ using an expression for the mean density following the Bray–Moss–Libby formulation [25] as $\bar{\rho}=\rho_0/(1+\tau\tilde{c})$ yields:

$$\rho_0\frac{\partial\tilde{u}_k}{\partial x_k}+\tau\frac{\partial(\bar{\rho}\,\widetilde{u_j''c''})}{\partial x_j}+2\tau\rho D\langle\kappa_m\rangle_s\Sigma = \tau\langle\rho(S_r+S_n)\rangle_s\Sigma\approx\tau\rho_0 S_L\Sigma \tag{7}$$

where $\langle Q\rangle_s$ is a surface averaged value of a general quantity Q given by: $\langle Q\rangle_s=\langle Q\Sigma'\rangle/\Sigma$ [10], and Eq. (6) has been incorporated. From recent DNS results [11,19,25], it is reasonable to assume that $\langle\rho(S_r+S_n)\rangle_s\approx\rho_0 S_L$. Using further Bray–Moss–Libby relations [25] the first term in Eq. (7) can be scaled as $\rho_0\partial\tilde{u}_k/\partial x_k\sim\rho_0\tau S_L\partial\tilde{c}/\partial r$, and consequently the peak location of $\rho_0\partial\tilde{u}_k/\partial x_k$ is close to the middle of the flame brush. An increase in u'/S_L leads to higher degree of gradient-type transport [26] and so the second term in Eq. (7) becomes a sink on the unburned side and source on the burned side. Recent DNS results for kernels [20] suggest that κ_m and $|\nabla c|$ are negatively correlated and so for large-radius kernels the effect of $2\tau\rho D\langle\kappa_m\rangle_s\Sigma$ is weak compared to the other terms in Eq. (7). For kernels the mean curvature is positive throughout [17] and hence so is $2\tau\rho D\langle\kappa_m\rangle_s\Sigma$. For large u'/S_L the flame becomes highly wrinkled with roughly equal positive and negative curvatures, thus reducing the mean value of κ_m [17]. The combined effect of these three mechanisms acts to determine the location of peak FSD value.

In Fig. 2 the maximum value of FSD is seen to decrease with increasing u'/S_L for both experimental and DNS data, with the length scale ratio L_{11}/δ_L remaining constant. This observation is supported by some previous experimental studies [27–29], although not by all [30]. This is believed to be the first time that the effect has been seen in DNS data, but some previous DNS studies (e.g., [31,32]) have reported the opposite trend. Thus, the exact conditions under which the peak FSD increases or decreases with u'/S_L is still an open question. Some insight can be gained by examining the modelled FSD transport equation [3]:

$$\frac{\partial\Sigma}{\partial t}+\frac{\partial(\tilde{u}_j\Sigma)}{\partial x_j}=\frac{\partial}{\partial x_i}\left(\frac{\nu_t}{\sigma_c}\frac{\partial\Sigma}{\partial x_i}\right)+\underbrace{(\delta_{ij}-\langle N_iN_j\rangle_s)\frac{\partial\tilde{u}_i}{\partial x_j}\Sigma}_{K_m} + \underbrace{\left\langle(\delta_{ij}-N_iN_j)\frac{\partial u_i''}{\partial x_j}\right\rangle_s\Sigma}_{K_t}+S_1+D_1 \tag{8}$$

where ν_t/σ_c is the ratio between the turbulent diffusion coefficient and Prandtl number, $S_1=-\nabla\cdot(\langle S_d\vec{N}\rangle_s\Sigma)$ and $D_1=\langle S_d\nabla\cdot\vec{N}\rangle_s\Sigma$. The second and third terms on the right hand side

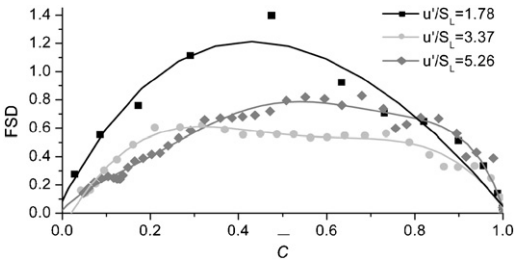

Fig. 3. Flame surface density evaluated from the 3D DNS flame kernels corresponding to methane–air flames of different turbulence intensity.

act as source terms, with K_t generally larger than K_m. The term K_t is given by $K_t = C_1 u'(1 + C_2 Da)/L_{11}$ [32] where C_1 and C_2 are model constants. The term S_1 is positive on the unburned side and negative on the burned side [3,6,11,12], while D_1 acts as a sink term throughout. According to Eq. (6) the term D_1 can be written as:

$$D_1 = D_{11} + D_{12} = \langle (S_r + S_n)\nabla \cdot \vec{N} \rangle_s \Sigma - 4D\langle \kappa_m^2 \rangle_s \Sigma \quad (9)$$

After normalising Eq. (9) by the Kolmogorov length η and velocity v_η scales following Peters [1] the term D_1 can be shown to scale with $Ka^{-1/2}$ where Ka is the Karlovitz number given by $Ka = v_\eta^2/S_L^2$. For the same scaling the term $D_{12} \sim (\rho D/\mu)^{-1} = Sc^{-1} \sim 0.7^{-1}$ is of order unity for methane–air flames and K_t scales as $Re_t^{-1/2} \sim Da^{-1}Ka^{-1}$. Hence, in equilibrium between sources and sinks, the maximum value of FSD scales as $Da^{-1}Ka^{-1/2}$ when $Ka < 1$ and as $Da^{-1}Ka^{-1}$ when $Ka > 1$ and so is determined by competition between the effects of Da and Ka. Clearly this hypothesis requires more careful analysis, which is beyond the scope of present study.

The variation of FSD with $\bar{c}$ for three-dimensional methane–air DNS is shown in Fig. 3. The peak in FSD is observed to shift towards the burned side with increasing u'/S_L. However, the maximum value of FSD obtained from two-dimensional and three-dimensional analysis can differ by a factor of up to two. It can also be seen on comparing Fig. 2d–f with Fig. 3 that the two-dimensional FSD profile shows greater scatter because the sample size is smaller than for the 3D case. It is also evident that, unlike the two-dimensional analysis, the three-dimensional analysis does not show a monotonic decrease of maximum FSD with increasing u'/S_L. This behaviour could be a further manifestation of competition between Da and Ka: an increase in u'/S_L for constant L_{11}/δ_L leads to a decrease (increase) in Da (Ka). A decrease in Da acts to increase the maximum FSD value, whereas an increase in Ka has the opposite effect. The observed differences between the values of FSD obtained from two-dimensional and three-dimensional analysis strongly motivate the development of three-dimensional measurement techniques in the future.

The experimental variation of FSD with $\bar{c}$ for lean hydrogen–air flames is shown in Fig. 4 (top row) for different values of u'/S_L. The FSD

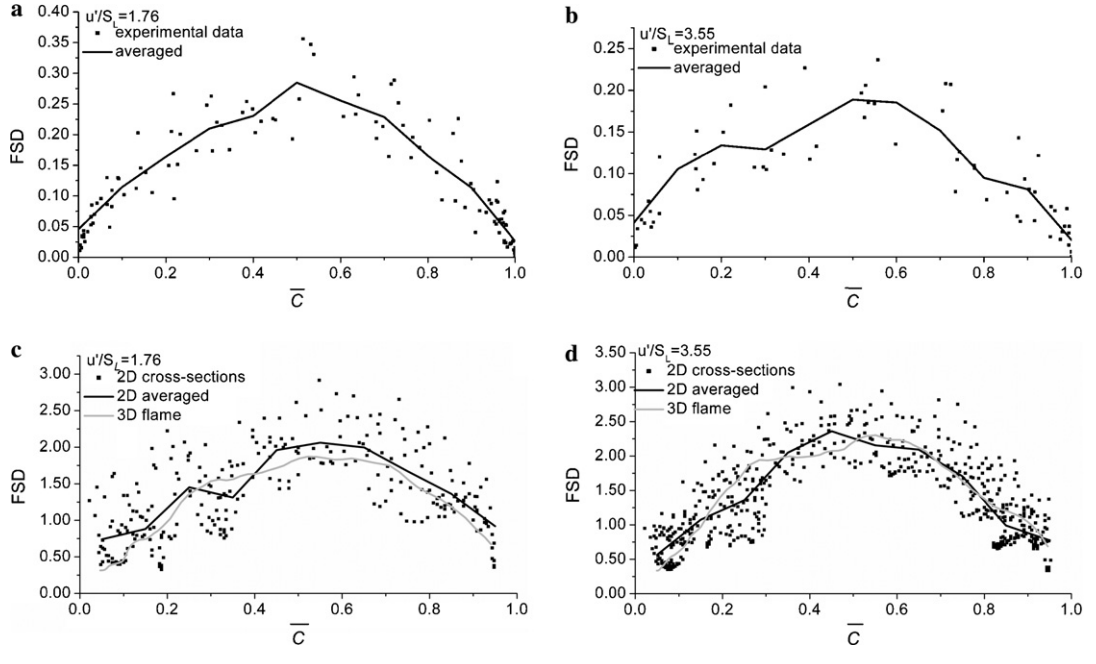

Fig. 4. Flame surface density of flames corresponding to lean hydrogen–air mixtures of different turbulence intensity (top row: experimental data; bottom row: DNS data).

distributions from two-dimensional and three-dimensional analyses of DNS data are presented in Fig. 4 (bottom row) for corresponding values of u'/S_L. It is evident that the peak FSD occurs close to $\bar{c} = 0.5$ for both experimental and two-dimensional DNS analysis. Comparing the FSD profiles for methane–air (Fig. 2) and hydrogen–air flames (Fig. 4) it is evident that the normalised FSD profiles remain similar for roughly equal values of u'/S_L, which is consistent with the measurements of Renou et al. [33]. However, the hydrogen–air cases show a more well-defined peak around $\bar{c} = 0.5$ than the higher turbulence methane–air cases.

For the hydrogen flames, the maximum value of FSD is also shown to decrease with u'/S_L for the experimental data, whereas both two-dimensional and three-dimensional analysis of DNS data predict an increase in maximum value of FSD with u'/S_L. This could be a manifestation of the difference in flame geometry between the experiment (spherical) and DNS (statistically planar), due to the negative correlation between $|\nabla c|$ and κ_m [12,20], and possibly different Lewis number effects on the $|\nabla c| - \kappa_m$ correlation [24] in the kernels in comparison to those in statistically planar flames. Moreover, the maximum values of the FSD from the two-dimensional analysis are found to be slightly larger than those from corresponding three-dimensional analyses. Again this motivates the need for experimental techniques which can offer 3D flame topology data [34] and which will allow for more complete comparisons with DNS. Also, the three-dimensional curvature of the kernel in the experimental case may have some significant effects which are missing in two dimensions. Clearly, more analysis is needed in order to resolve these issues, and the need for three-dimensional scalar field measurements is apparent.

6. Conclusions

The variation of FSD with Reynolds averaged reaction progress variable $\bar{c}$ has been analysed for stoichiometric methane–air and lean hydrogen–air flames by combining state-of-the-art imaging experiments and DNS. Similar post-processing techniques have been employed for extracting FSD values from both experimentally obtained OH-PLIF images and DNS data. The experimentally obtained FSD is compared with the FSD distribution obtained from both two-dimensional cross-sections of three-dimensional DNS data, and from three-dimensional analysis based on the gradient of the reduced reaction progress variable. It is found that the normalised FSD($\Sigma\delta_L$) distributions for methane–air and lean hydrogen–air flames are similar for comparable values of u'/S_L. For both flames the FSD distribution based on two-dimensional images of DNS data are found to be in good qualitative agreement with experimentally obtained FSD distributions. In the case of methane–air flames some FSD profiles are slightly skewed about $\bar{c} = 0.5$. By contrast, for lean hydrogen–air flames the maximum value of FSD is located close to $\bar{c} = 0.5$ for the u'/S_L values considered here both in experimental and simulated datasets. Maximum experimental values of FSD are found to decrease with u'/S_L which is consistent with experimental findings by other authors, however this is believed to be the first time that the effect has been seen in DNS data. The 2D analyses of DNS data for methane–air flames and experiment supports this, whereas an opposite trend is observed for hydrogen–air flames. For 3D FSD data obtained from DNS the trends are much different: overall the magnitude of the FSD is different from 2D data, and no monotonic decline in FSD maximum values were observed with increasing u'/S_L for methane–air flames. For hydrogen–air flames the maximum value of the FSD shows a monotonically increasing trend. It is proposed that a competition between Damköhler and Karlovitz number effects may provide an explanation for this behaviour. Possibly the effect is amplified by effects of mean flame radius and differential diffusion effects due to non-unity Lewis numbers. The work demonstrates the need for the development of more advanced 3D scalar measurement techniques in order to validate these hypotheses.

Acknowledgments

This work was supported by the EPSRC (J.H.—Advanced Research Fellowship; S.G.—CASE studentship; C.F.K.—PLATFORM grant), Rolls-Royce plc (S.G.), the German Academic Exchange Service (M.K.—DAAD Postdoc Program), and the Swedish Research Council (J.H.). We thank M. Aldén, A. Dreizler, U. Maas, and S. Lindenmaier for the joint collaboration and fruitful discussion.

References

[1] N. Peters, *Turbulent Combustion*, Cambridge University Press, Cambridge, 2000.
[2] S. Candel, T. Poinsot, *Combust. Sci. Tech.* 70 (1990) 1–15.
[3] R.S. Cant, S.B. Pope, K.N.C. Bray, *Proc. Combust. Inst.* 23 (1990) 809–815.
[4] K.N.C. Bray, P.A. Libby, *Combust. Flame* 61 (1985) 87–102.
[5] M. Boger, D. Veynante, H. Boughanem, A. Trouvé, *Proc. Combust. Inst* 27 (1998) 917–925.
[6] E.R. Hawkes, R.S. Cant, *Proc. Combust. Inst.* 28 (2000) 51–58.
[7] T. Mantel, R. Borghi, *Combust. Flame* 96 (1994) 443–457.

[8] R.O.S. Prasad, J.P. Gore, *Combust. Flame* 116 (1999) 1–14.
[9] S.B. Pope, W.K. Cheng, *Proc. Combust. Inst.* 22 (1988) 781–789.
[10] H.G. Weller, C.J. Marooney, A.D. Gosman, *Proc. Combust. Inst.* 23 (1990) 629–636.
[11] A. Trouvé, T.J. Poinsot, *J. Fluid Mech.* 278 (1994) 1–32.
[12] N. Chakraborty, R.S. Cant, *Phys. Fluids* 17 (65108) (2005) 1–15.
[13] D. Veynante, J.M. Duclos, J. Piana, *Proc. Combust. Inst.* 25 (1994) 1249–1256.
[14] C.J. Lawn, T.C. Williams, R.W. Schefer, *Proc. Combust. Inst.* 30 (2005) 1749–1756.
[15] D. Bradley, R.A. Hicks, M. Lawes, C.G.W. Sheppard, R. Woolley, *Combust. Flame* 115 (1998) 126–144.
[16] C.F. Kaminski, J. Hult, M. Alden, et al., *Proc. Combust. Inst.* 28 (2000) 399–405.
[17] S. Gashi, J. Hult, K.W. Jenkins, N. Chakraborty, S. Cant, C.F. Kaminski, *Proc. Combust. Inst.* 30 (2005) 809–817.
[18] S. Lindenmaier, Zeitaufgelöste Laser-diagnostische Untersuchung der Funkenzündung, PhD thesis, University of Stuttgart, Stuttgart, Germany, 2001.
[19] N. Chakraborty, R.S. Cant, *Combust. Flame* 137 (2004) 129–147.
[20] K.W. Jenkins, M. Klein, N. Chakraborty, R.S. Cant, *Combust. Flame* 145 (2005) 415–434.
[21] J.F. Driscoll, A. Gulati, *Combust. Flame* 72 (1988) 31–152.
[22] R.K. Cheng, I.G. Shepherd, L. Talbot, *Proc. Combust. Inst.* 22 (1988) 771–780.
[23] T.C. Chew, K.N.C. Bray, R.E. Britter, *Combust. Flame* 80 (1990) 65–82.
[24] N. Chakraborty, R.S. Cant, *Phys. Fluids* 17 (105105) (2005) 1–20.
[25] K.N.C. Bray, P.A. Libby, J.B. Moss, *Combust. Flame* 61 (1985) 87–102.
[26] D. Veynante, A. Trouvé, K.N.C. Bray, T. Mantel, *J. Fluid Mech.* 332 (1997) 263–293.
[27] F.O. Young, R.W. Bilger, *Combust. Flame* 109 (1997) 683–700.
[28] Y.-C. Chen, M.S. Monsour, *Proc. Combust. Inst.* 27 (1998) 811–818.
[29] Y.-C. Chen, R.W. Bilger, *Combust. Flame* 131 (2002) 400–435.
[30] A. Soika, F. Dinkelacker, A. Leipertz, *Proc. Combust. Inst.* 27 (1998) 785–792.
[31] C. Rutland, R.S. Cant, in: Proceedings of Summer Program, Centre of Turbulence Research, NASA Ames/Stanford University, 1994, pp. 75–94.
[32] N. Swaminathan, K.N.C. Bray, *Combust. Flame* 143 (2005) 549–565.
[33] B. Renou, A. Mura, E. Samson, A. Boukhalfa, *Combust. Sci. Technol.* 174 (4) (2002) 143–179.
[34] J. Hult, B. Axelsson, A. Omrane, et al., *Exp. Fluids* 33 (2002) 265–269.